

Pressure (mechanical) effects in infrared tissue ablation

Glenn Edwards,^{*,a} Wolfgang Wagner,^a Adam Sokolow,^a and Robert Pearlstein^b

^aPhysics Department, Duke University, Durham, NC USA 27708;

^bDepartment of Surgery, Duke University Medical Center, Durham, NC USA 27710

ABSTRACT

We experimentally demonstrate that the acoustic transients propagating as a result Free-Electron Laser (FEL) ablation in brain tissue exhibit a strong FEL wavelength dependence. These acoustic transients were measured with a time-resolved, polarization quadrature laser interferometer. The transients are multiphased, with displacements of tens of microns and durations of tens of milliseconds. We calculated the Fourier transforms, power spectra, and pressure transients based on these displacement data sets. For 3.0 μm irradiation, the bandwidth of the Fourier components extends to ~ 20 kHz, while for 6.45 μm irradiation the bandwidth of the Fourier components extend to ~ 8 kHz. For the 3.0 μm irradiation, the power spectra indicate acoustic energy propagates in the bandwidth up to ~ 12 kHz, with structure in the 1-4 kHz range. For the 6.45 μm radiation, the mechanical power spectra indicate the acoustic energy propagates in the bandwidth up to ~ 7 kHz, with structure throughout. The pressure transients resulting from 3.0 μm irradiation have a leading phase with a faster onset, shorter duration, and more than ten times the peak pressure compared to that observed in pressure transients resulting from 6.45 μm irradiation. For 3.0 μm irradiation, the observed pressure transients have peak pressures in the MPa range and durations of ~ 1 ms, while for 6.45 μm irradiation the pressure transients have peak pressures in the 0.1 MPa range and durations of about ~ 3 ms.

Keywords: Tissue ablation; mechanical effects; interferometry

1. INTRODUCTION

There are three reasons for our interest in the mechanical effects associated with tissue ablation resulting from irradiation with short-pulsed lasers operating in the mid-infrared wavelength range. First, the infrared Mark-III Free-Electron Laser (FEL) has been used successfully for human brain surgery and animal ophthalmic surgery [1]. The FEL, when tuned to wavelengths near 6.45 μm , offers key surgical advantages over lasers operating near 3.0 μm and UV and visible wavelengths as well. While the 3.0 μm wavelength can lead to very rapid heating of tissue water, wavelengths in the 5.9-to-6.6 μm band can lead to very rapid heating of both tissue water and tissue proteins. Extensive experimentation has demonstrated the advantage of wavelengths in the 5.9-to-6.6 μm band relative to the 3.0 μm wavelength in limiting collateral damage for surgical applications, which has been accounted for in terms of photothermal effects, chemical kinetics, and mechanical effects [2,3]. To support human surgical applications, one Mark-III FEL at Vanderbilt University was upgraded from a research laser to qualify as a medical laser and indeed has performed impressively as a tool for human surgery [1]. The FEL was tuned to 6.45 μm for human neurosurgery, where that choice in wavelength was based on an assessment of both collateral damage and ablation yield. Medical acceptance of the FEL has been limited, however, due to its complexity, size, and cost. Consequently, there has been interest and some progress towards the development of alternative infrared medical laser technology that would be relatively compact and inexpensive. This interest highlighted the need to better understand both how much flexibility there is in the choice of wavelength in the 5.9-to-6.6 μm range, since candidate laser technologies tend not to be tunable sources, and the role of the FEL superpulse structure in the ablation process, since a GHz repetition rate, picosecond laser likely excludes conventional laser technologies. With regard to identifying the operational wavelength for the alternative laser technology, there are tissue specific effects when considering only collateral damage, where the FEL wavelengths that minimized collateral

*Edwards@fel.duke.edu; phone (919) 660 2674; fax (919) 660 2671

damage were 6.45 μm for brain, 6.0 μm for corneal stroma, and all wavelengths tested in the 6.0-to-6.45 μm range for dermis [4]. However, given the challenge of reproducing the average power produced by the Mark-III FEL to achieve an acceptable ablation rate, both ablation yield and collateral damage warrant consideration. Based on these two criteria, our attention focused on the 6.45 μm wavelength. With regard to pulse structure, a key step towards the development of alternative medical laser technology was the recognition that the superpulse structure of the Mark-III FEL could be relaxed and, specifically, biophysical modeling led to the prediction that replacing the superpulse with the more technologically forgiving nanosecond pulse train would produce comparable ablative results that maintain the surgical advantages [5]. Such a laser was developed and experimentally demonstrated that a nanosecond laser operating at 6.45 μm produces minimal collateral damage in rat brain tissue analogous to that seen with the Mark-III FEL; however, the average power for this nanosecond laser is insufficient to satisfy the ablation rate required for surgical applications [6]. Efforts are underway to increase the average power by three orders of magnitude to exceed that requirement for ablation rate, once again highlighting the importance of both ablation yield and collateral damage. As various wavelengths and pulse structures are tested, it is important to consider the consequences for the onset of collateral damage, including the contribution due to mechanical effects.

The second, closely related, reason for our interest in mechanical effects in mid-infrared tissue ablation is our interest in understanding the ablative mechanism at a more fundamental level. In the past, we have developed a semi-quantitative, semi-phenomenological biophysical model based on heat transfer and chemical kinetics that describes the onset of the ablation process, which to its credit was the basis for quantitatively predicting how to relax the constraint on the superpulse structure that was experimentally verified. A key feature of the model is the very fast time scale for the onset of infrared tissue ablation with the Mark-III FEL, where the thermodynamic instability that results in explosive vaporization of tissue water is reached in ~ 10 ns. In parallel, and apparently key to the wavelength dependence, is the similarly very rapid heating of tissue protein. While the thermodynamic instability of water is fundamentally understood, little is known about heating protein on this time scale. This is an unresolved, fundamental issue. Our model extrapolated known chemical kinetics determined at substantially longer time scales to the nanosecond regime. A more fundamental understanding of the mechanism for collateral damage and its infrared wavelength dependence requires an investigation of the photo-thermal-mechanical mechanism throughout the full time course of ablation, a harrowing theoretical/modeling challenge once explosive vaporization commences. Consequently we have interests in developing a foundation of experimental data that address this unresolved, fundamental issue throughout the time course of ablation and, more specifically, have become interested in time-resolved measurements of acoustic transients.

The third reason for our interest in mechanical effects in mid-infrared tissue ablation is based on several observations under experimental conditions that highlight pressure wave propagation. We have observed that the damage pattern following tissue ablation with 3.0 μm irradiation mimics that seen in brain trauma due to high velocity projectiles. We also have observed a breakdown in the blood brain barrier in a large zone extending beyond what we typically have identified as the region of collateral damage under experimental conditions that suggest pressure wave propagation. Furthermore, we observed that the ablation cavities caused by 6.45 μm irradiation tend to extend to the interface between the mechanically “soft” grey matter and the mechanically “stiff” white matter. In total, these observations resulted in taking a closer look at mechanical effects.

The following is a preliminary report of acoustic transients measured during FEL ablation due a single macropulse at an infrared wavelength of either 3.0 or 6.45 μm . Here we emphasize a comparison of the two wavelengths. Initially we attempted an experimental approach using a piezoelectric transducer based on PVDF films, where we anticipated that we would be able to account for the nonlinear response. This was not realized due to the fundamental limitations of PVDF technology, so we turned our attention to an interferometric approach.

2. METHODS

We have developed an interferometer-based method to measure the displacement of the bottom surface of a tissue slice following irradiation of the top surface with a single FEL macropulse, where this instrument has exceptionally large bandwidth (150 MHz) (Figure 1). The interferometer essentially counts intensity fringes, so there is an inherent ambiguity as to the direction of motion, which leads to the unwrapping problem that plagues processing these data into

plots of displacement of the bottom tissue surface as a function of time. To minimize the confounding effects of this unwrapping ambiguity, we implemented quadrature detection, where the displacement-encoded wave is interferometrically combined with two quadrature (90 degrees) shifted reference waves, *i.e.*, two channels of information containing the interference signal and, in effect, the derivative of the interference signal [7]. When the superposition of the translated and reference waves are split by polarization into two photodetectors, the displacement-dependent signal on each detector is offset by a 90 degree phase lag. Thus in practice we can remove the ambiguity and unwrap most data sets resulting in plots of displacement of the bottom tissue surface as a function of time.

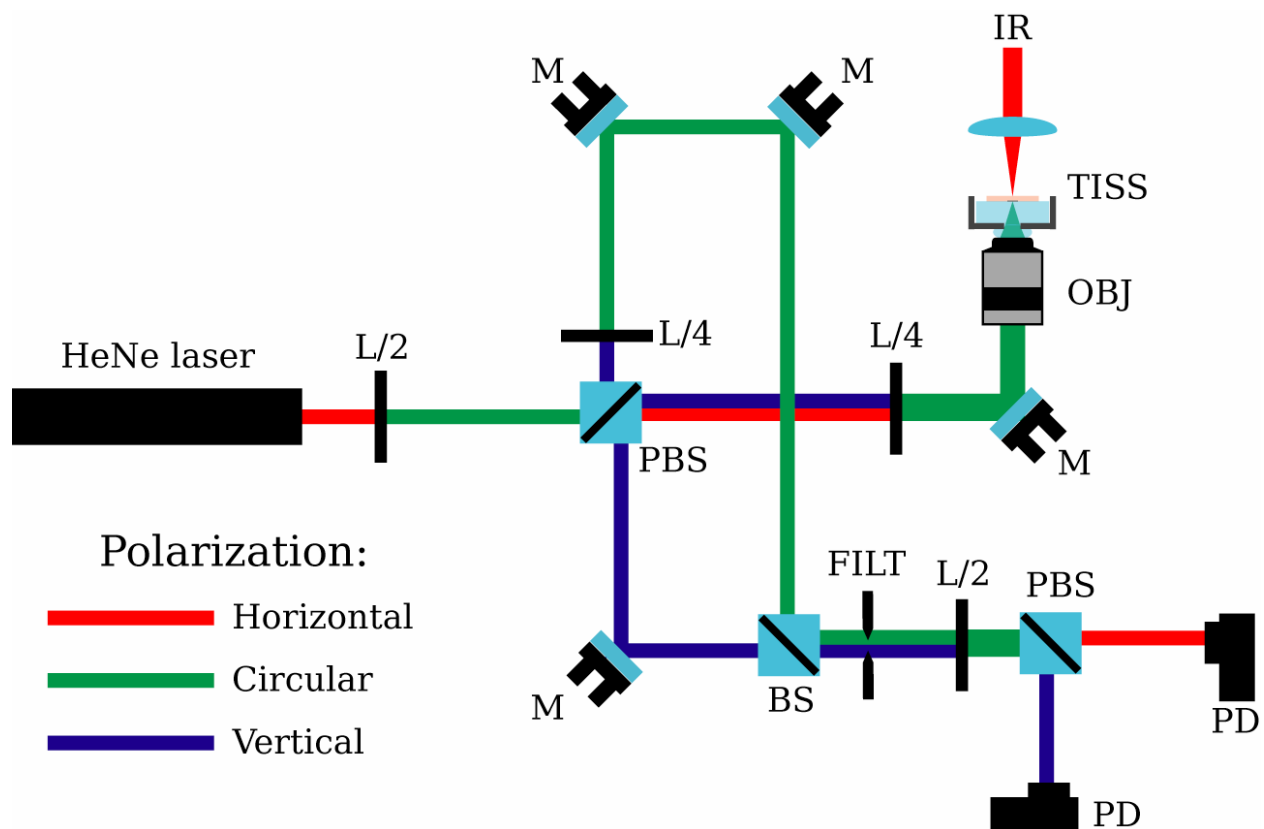


Figure 1. Light from a Uniphase 1125P HeNe laser is split by a polarizing beam splitter (PBS) into vertical and horizontal polarized beams, according to a half wave-plate ($L/2$). The horizontal beam from the PBS is made circular by a quarter wave-plate ($L/4$) and sent to the tissue sample. Light which is reflected is rotated to a vertical polarization by the quarter wave-plate and sent towards the detectors by the PBS. The reference beam is converted to circular polarization with a quarter wave-plate ($L/4$), and combined with the vertically polarized light from the laser. The resulting beams are spatially filtered (FILT), and the vertical beam is transformed into a 45 degree polarization by a half-wave plate ($L/2$). A polarizing beam-splitter (PBS) splits the interfering vertical and horizontal components of the two beams onto two photodetectors (PD).

Brains from Sprague-Dawley rats were sliced into 1.5 mm thick coronal sections and kept frozen in dry ice until just before the experiment, when they were returned to room temperature. A retroreflector was then placed on the bottom surface of the tissue slice. More specifically, one square millimeter of 1 mil aluminum foil, which previously had been sprayed with retroreflective paint (Krylon Reflect-A-Lite), was located on the bottom surface of the tissue, reflective side down.

To mount the tissue sample (Figure 2), first a 1 cm thick ultrasound gel pad (Aquaflex ultrasound gel pads, 2cmX9cm diameter) was placed in its holder (that has a 5/8" hole), directly above the microscope objective (10X DIN 0.25, Edmund Optics). The tissue sample was then mounted and ultrasound gel (AQUASONIC Clear Ultrasound Gel) was

injected to span any space between the gel pad and the bottom tissue surface. Both the ultrasound gel pads and the ultrasound gel are optically transparent and acoustic-impedance matched to brain tissue. Height (z) adjustment positioned the bottom tissue surface/retroreflector in the focus of the objective and focal plane (x, y) adjustment optimized the retro-reflection into the interferometer. The laser interferometer is self-calibrating. For instrument validation prior to FEL-based studies, we ablated samples using a Minilite-II laser that delivers 1064nm pulses with energies of 25 mJ and durations of 5 ns.

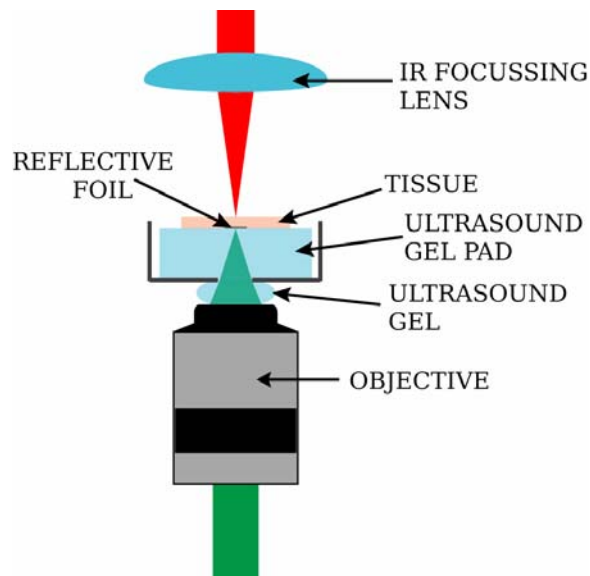


Figure 2. Tissue sample mounting -- an expanded view of the components in the upper-right hand corner of Figure 1.

The IR focusing lens (Figure 2) focused the infrared FEL beam to a spot size of ~50 microns for 3.0 μm irradiation and ~75 microns for 6.45 μm FEL irradiation. For both wavelengths, each macropulse ablated tissue. We collected displacement data from the quadrature interferometer through the two amplified 150 MHz photodetectors (PDA10A, Thorlabs), which determines the overall bandwidth. For each ablation event, the oscilloscope records 5 million points during 10 milliseconds of the acoustic transient. The signals are stored in binary form on a hard disk connected by USB to the oscilloscope (Maxtor Personal Storage 3200) for subsequent processing. These data were processed by normalizing the two photodetector traces to produce wrapped data sets, which were then unwrapped into displacement traces. Fourier transforms and power spectra were calculated in MatLab. Pressure transients were determined using the expression $\Delta P = -B \Delta V / V_0$, where ΔP is the change in pressure, ΔV is the change in volume, V_0 is the initial volume, and B is bulk modulus for brain tissue. This research was carried out at Duke University's FEL Laboratory and Vanderbilt University's FEL Center.

3. RESULTS

For all figures in the results section, we superpose five sequential acoustic transients that have propagated from the bottom of the ablation cavity on the top tissue surface, through the tissue, to the bottom tissue surface. The FEL was focused to a given spot on the top tissue surface and a single macropulse was delivered. This was repeated four additional times at the same x-y location. The first macropulse results in the black trace, followed by red, blue, green and purple traces.

3.1 Displacements

Figure 3 presents the displacement of the bottom surface of the tissue following a 2mJ (left) or 2.5 mJ (right) macropulse of 3.0 μm FEL irradiation at the top surface of the tissue. The acoustic transients have been plotted such that the arrival of the leading edge of the acoustic transient occurs at 0.48 ms, an arbitrary time due to triggering by the oscilloscope. Positive displacement corresponds to movement towards the interferometer. In general, the tissue abruptly moves towards the interferometer, swings back and more slowly moves away from the interferometer, followed by some reverberation. With increasing macropulse energy, the magnitude of the displacement increases and there is an indication that the acoustic transient becomes more complex.

Figure 4 presents the displacement data following irradiation with either a 4mJ (left) or a 5.0mJ (right) macropulse at 6.45 μm . The acoustic transients exhibit more phases and were not completely over at 10 ms. Comparing Figures 3 and 4, it is apparent that there is a strong wavelength dependence to the displacement data. The displacements at 6.45 μm are less than half that seen at 3.0 μm .

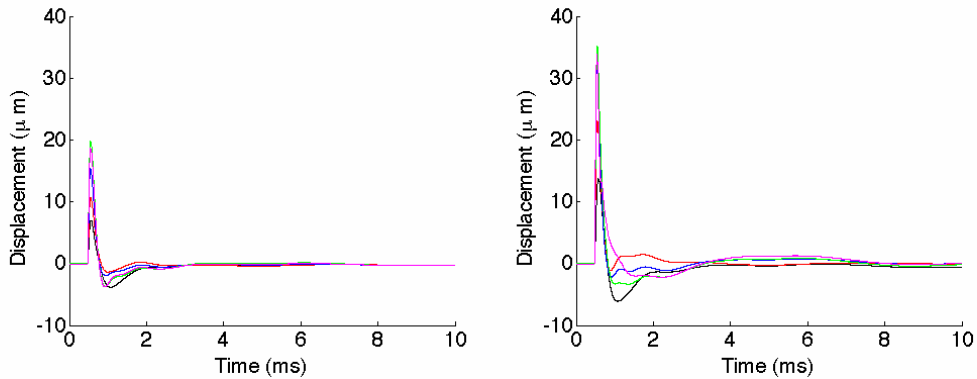


Figure 3. Displacements of bottom tissue surface following 3.0 μm FEL irradiation. Tissue is 1.5 mm thick. Left) 2 mJ delivered in a single macropulse. Right) 2.5 mJ delivered in a single macropulse.

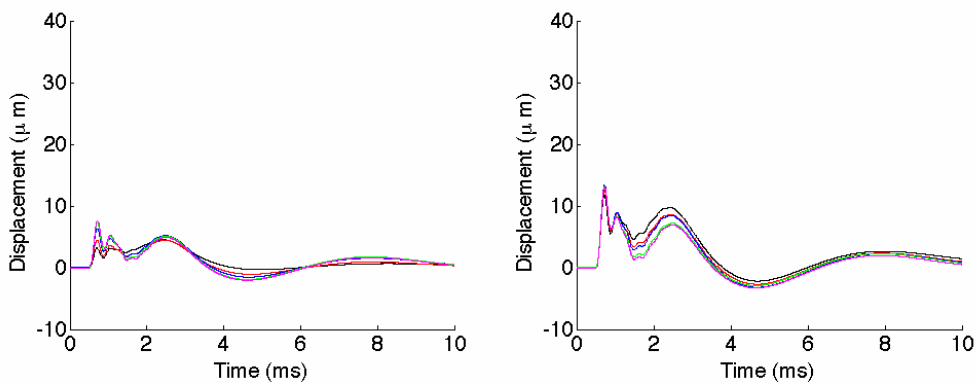


Figure 4. Displacements of bottom tissue surface following 6.45 μm FEL irradiation. Tissue is 1.5 mm thick. Left) 4 mJ delivered in a single macropulse. Right) 5 mJ delivered in a single macropulse.

To investigate further the wavelength dependence in the displacement traces, in Figures 5 and 6 we replot the displacement data at an expanded time scale. It is apparent that the leading edge of the acoustic transient due to $3.0\ \mu\text{m}$ irradiation is more abrupt than that due to $6.45\ \mu\text{m}$ irradiation. This indicates that higher frequency content is present in the acoustic transient due to $3.0\ \mu\text{m}$ irradiation relative to $6.45\ \mu\text{m}$ irradiation, as will be calculated in the next section. It is apparent that the duration of the initial phase is shorter following $3.0\ \mu\text{m}$ irradiation relative to $6.45\ \mu\text{m}$ irradiation. It also is apparent that the magnitude of the displacements may correlate with the sequence of macropulses (black, red, blue, green, then purple), where the depth of the ablation cavity due to a single macropulse is a very small fraction of $1.5\ \text{mm}$.

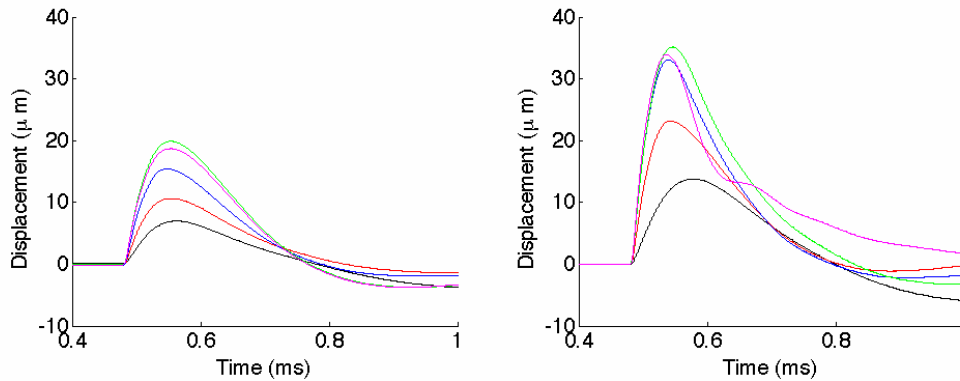


Figure 5. Displacements of bottom tissue surface following $3.0\ \mu\text{m}$ FEL irradiation. This is an expanded time scale image of Fig. 3, emphasizing the onset of displacement. Tissue is $1.5\ \text{mm}$ thick. Left) $2\ \text{mJ}$ delivered in a single macropulse. Right) $2.5\ \text{mJ}$ delivered in a single macropulse.

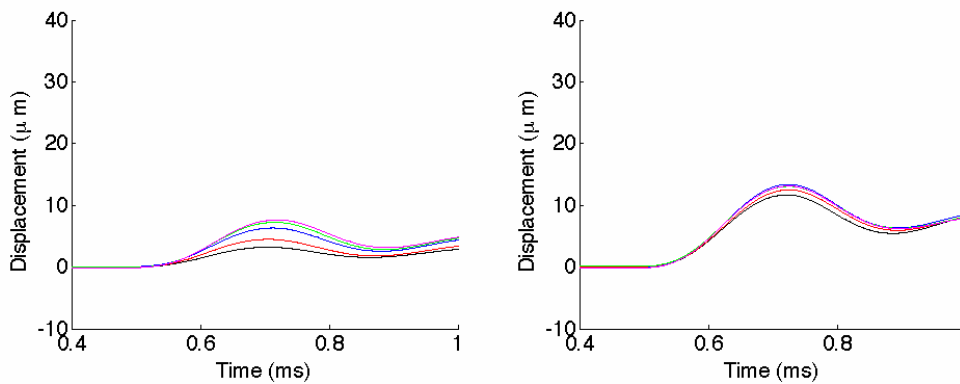


Figure 6. Displacements of bottom tissue surface following $6.45\ \mu\text{m}$ FEL irradiation. This is an expanded time scale image of Fig. 4, emphasizing the onset of displacement. Tissue is $1.5\ \text{mm}$ thick. Left) $4\ \text{mJ}$ delivered in a single macropulse. Right) $5\ \text{mJ}$ delivered in a single macropulse.

3.2 Fourier transforms and power spectra

Given this wavelength dependence in the displacement associated with these acoustic transients, we now quantify the Fourier content. Figures 7 and 8 present the Fourier transform for the displacement data shown in Figures 3 and 4. The bandwidth at $3.0\ \mu\text{m}$ FEL irradiation extends to $\sim 20\ \text{kHz}$, while that at $6.45\ \mu\text{m}$ FEL irradiation extends to $\sim 8\ \text{kHz}$. In addition, at either FEL wavelength the amplitudes of the Fourier components increase with macropulse energy. To investigate any wavelength dependent structure in the Fourier content, Figure 9 replots Figure 7 on an expanded scale for

comparison with Figure 8. For $3.0\ \mu\text{m}$ irradiation, we see structure at $\sim 380\ \text{Hz}$ and $\sim 1.3\ \text{kHz}$, while for $6.45\ \mu\text{m}$ irradiation, we see structure at $\sim 1\ \text{kHz}$, $\sim 3.6\ \text{kHz}$, and $\sim 5.9\ \text{kHz}$. While the structure evident in the $6.45\ \mu\text{m}$ data sets presented in Figure 8 extends to higher frequency than the structure evident in the $3.0\ \mu\text{m}$ data sets presented in Figure 7, there is substantial unresolved background in the Fourier content presented in the $3.0\ \mu\text{m}$ data presented in Figures 7 and 9, extending to $\sim 25\ \text{kHz}$. Apparently this unresolved background accounts for the sudden onset seen in the displacement data sets shown in Figure 4.

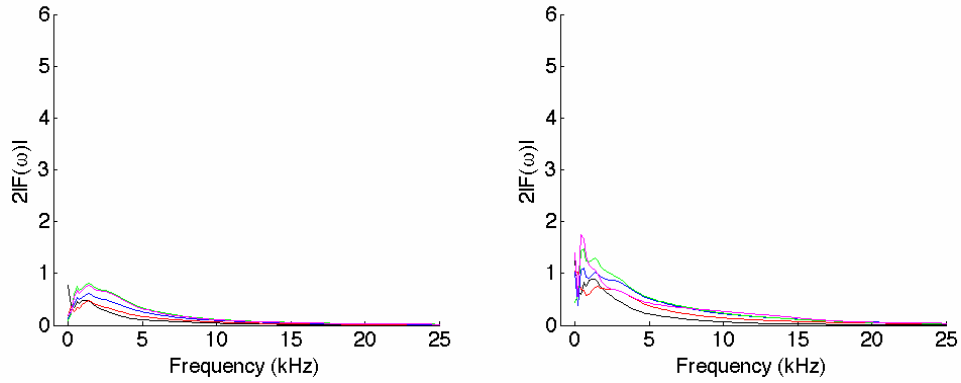


Figure 7. Fourier transforms of the displacements of the bottom tissue surface following $3.0\ \mu\text{m}$ FEL irradiation. Tissue is $1.5\ \text{mm}$ thick. Left) $2\ \text{mJ}$ delivered in a single macropulse. Right) $2.5\ \text{mJ}$ delivered in a single macropulse.

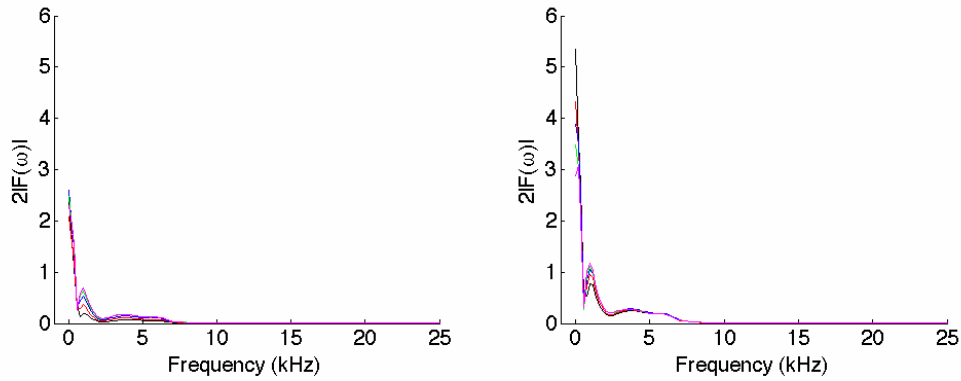


Figure 8. Fourier transforms of the displacements of bottom tissue surface following $6.45\ \mu\text{m}$ FEL irradiation. Tissue is $1.5\ \text{mm}$ thick. Left) $4\ \text{mJ}$ delivered in a single macropulse. Right) $5\ \text{mJ}$ delivered in a single macropulse.

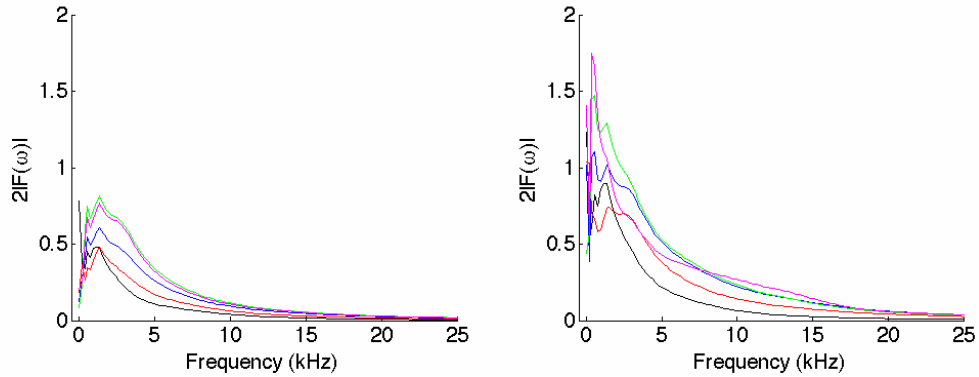


Figure 9. Fourier transforms of the displacements of the bottom tissue surface following $3.0\ \mu\text{m}$ FEL irradiation. The amplitudes of the Fourier components are presented on an expanded time scale to highlight apparent structure in the acoustic transient. Tissue is 1.5 mm thick. Left) 2 mJ delivered in a single macropulse. Right) 2.5 mJ delivered in a single macropulse.

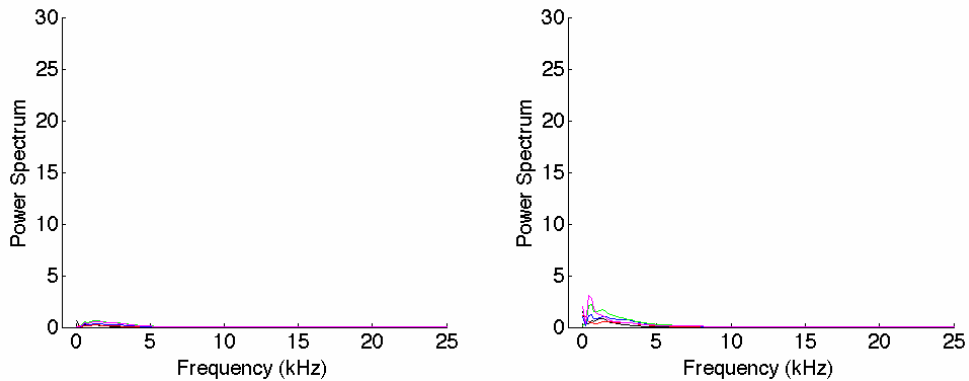


Figure 10. Power spectra of the displacements of the bottom tissue surface following $3.0\ \mu\text{m}$ FEL irradiation. Tissue is 1.5 mm thick. Left) 2 mJ delivered in a single macropulse. Right) 2.5 mJ delivered in a single macropulse.

Next we calculated the power spectra to determine which acoustic frequencies survive as the acoustic transient propagates 1.5 mm into the tissue. Figures 10 and 11 present the power spectra for the displacement data sets shown in Figures 3 and 4. For comparison with the Fourier transform data sets, we first plot the power spectra through 25 kHz, then replot these power spectra on expanded scales in Figures 12 and 13. For each FEL wavelength, the power in a Fourier component increases with macropulse energy. For $6.45\ \mu\text{m}$ FEL irradiation, the acoustic power is primarily carried by Fourier components at or below ~ 1 kHz, with a resolved feature centered near 1 kHz, and an unresolved contribution below ~ 600 Hz. In contrast, for $3.0\ \mu\text{m}$ FEL irradiation the power is carried by Fourier components extending beyond 12 kHz, with resolved features centered near 380 Hz, 570 Hz, and 1.3 kHz and a partially resolved feature centered near 2.6 kHz.

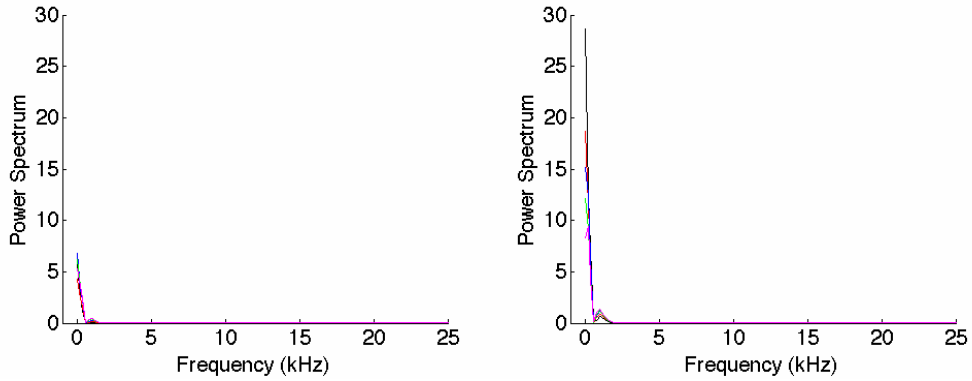


Figure 11. Power spectra of the displacements of bottom tissue surface following 6.45 μm FEL irradiation. Tissue is 1.5 mm thick. Left) 4 mJ delivered in a single macropulse. Right) 5 mJ delivered in a single macropulse.

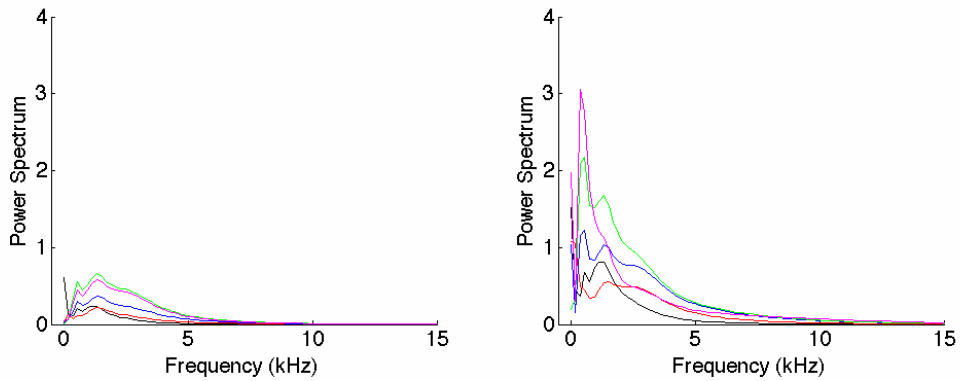


Figure 12. Power spectra of the displacements of the bottom tissue surface following 3.0 μm FEL irradiation. Both axes are presented on an expanded time scale to highlight apparent structure in the acoustic transient. Tissue is 1.5 mm thick. Left) 2 mJ delivered in a single macropulse. Right) 2.5 mJ delivered in a single macropulse.

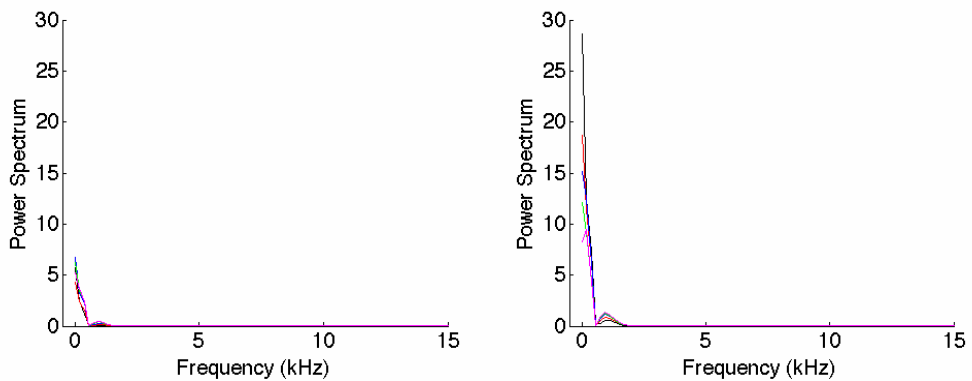


Figure 13. Power spectra of the displacements of bottom tissue surface following 6.45 μm FEL irradiation. Both axes are presented on an expanded time scale to highlight apparent structure in the acoustic transient. Tissue is 1.5 mm thick. Left) 4 mJ delivered in a single macropulse. Right) 5 mJ delivered in a single macropulse.

3.3 Pressure transients

Figures 14 and 15 present the pressure transients calculated from the displacement data sets presented in Figures 3 and 4. For $3.0\ \mu\text{m}$ FEL irradiation, there is an impulsive leading pressure rise, followed by a longer phase of pressure decrease. The peak pressures are in the megaPascal range and the pressure transients last less than a millisecond. For $6.45\ \mu\text{m}$ FEL irradiation, the pressure transients are strikingly smaller and slower. As a qualitative comparison, while the $6.45\ \mu\text{m}$ micron pressure transient seems nearly elastic, the impulsive leading phase of the $3.0\ \mu\text{m}$ pressure transients may be indicative of non-linear or possibly shock-wave effects. To demonstrate the abrupt onset of the $3.0\ \mu\text{m}$ pressure transient, Figures 16 and 17 replot these data sets on expanded time scales. Note that the data points are spaced by $10\ \text{ns}$.

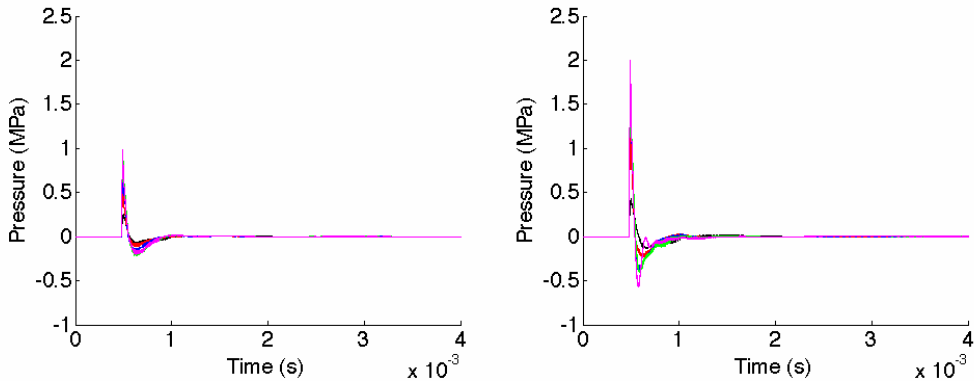


Figure 14. Pressure transients of bottom tissue surface following $3.0\ \mu\text{m}$ FEL irradiation. Tissue is $1.5\ \text{mm}$ thick. Left) $2\ \text{mJ}$ delivered in a single macropulse. Right) $2.5\ \text{mJ}$ delivered in a single macropulse.

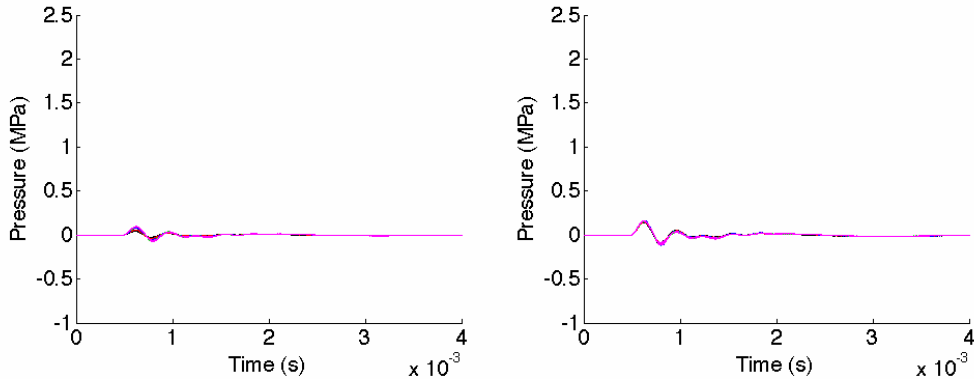


Figure 15. Pressure transients of bottom tissue surface following $6.45\ \mu\text{m}$ FEL irradiation. Tissue is $1.5\ \text{mm}$ thick. Left) $4\ \text{mJ}$ delivered in a single macropulse. Right) $5\ \text{mJ}$ delivered in a single macropulse.

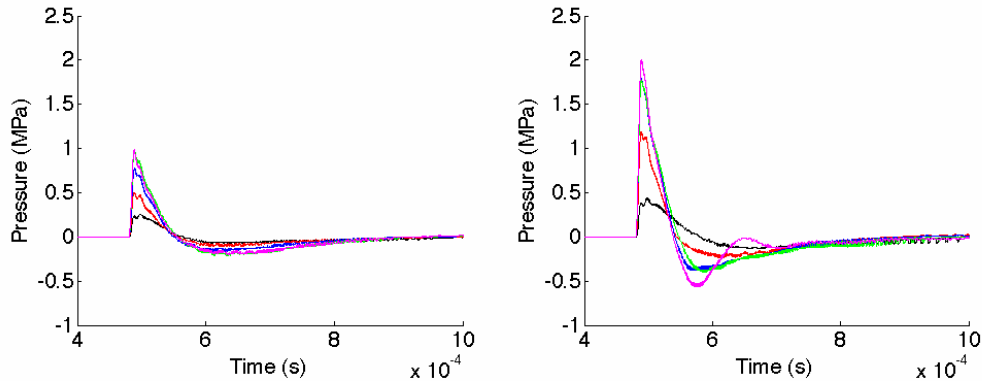


Figure 16. Pressure transients of bottom tissue surface following 3.0 μm FEL irradiation. This is an expanded time scale image of Fig. 14 to highlight the onset of the pressure transient. Tissue is 1.5 mm thick. Left) 2 mJ delivered in a single macropulse. Right) 2.5 mJ delivered in a single macropulse.

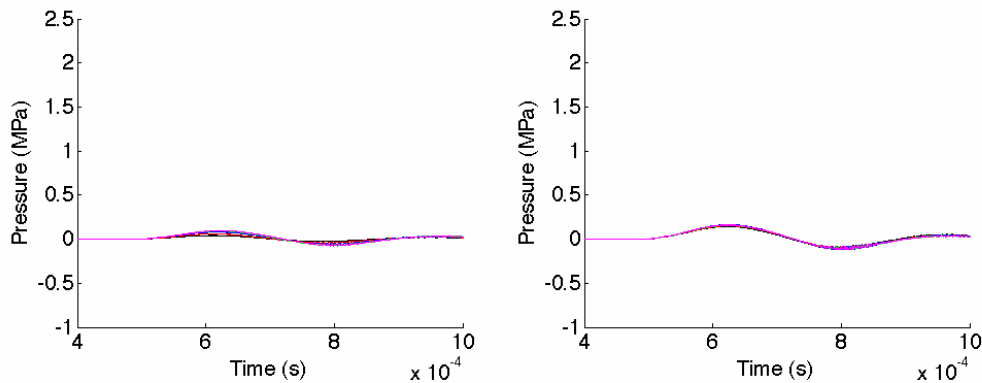


Figure 17. Pressure transients of bottom tissue surface following 6.45 μm FEL irradiation. This is an expanded time scale image of Fig. 15 to highlight the onset of the pressure transient. Tissue is 1.5 mm thick. Left) 4 mJ delivered in a single macropulse. Right) 5 mJ delivered in a single macropulse.

3. DISCUSSION

We have reported our experimental measurements where an FEL macropulse focused on the top surface of a brain tissue slice results in an acoustic transient that travels to the bottom surface. We have measured the displacement of the bottom surface, then based on these data calculated the Fourier transforms, power spectra, and pressure transients. The FEL wavelength of 6.45 μm targets heating to both tissue water and tissue protein, while the FEL wavelength of 3.0 μm targets heating to tissue water.

We observe multiphase acoustic transients with a strong wavelength dependence. For 3.0 μm irradiation, the leading phase of the acoustic transient is more pronounced and sudden relative to 6.45 μm irradiation, which we have quantified in terms of displacements, Fourier components, power in these components, and pressure transients. Most strikingly, the onset of the pressure transient due to 3.0 μm irradiation is impulsive, and an order of magnitude greater than what we observed with 6.45 μm irradiation. To quantitatively summarize our 3.0 μm irradiation measurements, we observe surface displacements of tens of microns with a dynamic range extending to tens of kHz, and peak pressures of megapascals. All are reduced for our 6.45 μm irradiation measurements.

4. CONCLUDING REMARKS

In the future, we will present a more systematic investigation of the propagation properties of these acoustic transients as a function of wavelength, tissue thickness, and macropulse energies. It remains a theoretical and modeling challenge to use these acoustic transients, offset by propagation through millimeters of brain tissue, as a signature for ablation dynamics. We are encouraged, however, by the strong wavelength dependencies exhibited in these data. Another challenge to be faced in the future is to place these results in the context of mechanisms for collateral damage and in the context of mechanisms for traumatic brain injury.

REFERENCES

- ^[1]Edwards, G.S., Austin, R.H., Carroll, F.E., Copeland, M.L., Couprie, M.E., Gabella, W.E., Haglund, R.F., Hooper, B.A. M.S. Hutson, Jansen, E.D., Joos, K.M., Kiehart, D.P., Lindau, I., Miao, J., Pratisto, H.S., Shen, J.H. Tokutake, Y., van der Meer, L. and Xie, A., "FEL-based-biophysical and biomedical instrumentation," *Review of Scientific Instruments* 74(7), 3207 (2003). See references therein.
- ^[2]Edwards, G.S., Allen, S.J, Haglund, R.F., Nemanich, R.J., Redlich, B., Simon, J.D., and Yang, W.-C., "Applications of Free-Electron Lasers in the Biological and Material Sciences," *Photochemistry and Photobiology* 81, 711-735 (2005). See references therein.
- ^[3]Mackanos, M.A., Kozub, J.A. and Jansen, E.D., "The effect of free-electron laser pulse structure on mid-infrared soft tissue ablation: ablation metrics," *Phys. Med. Biol.* 50, 1871-1883 (2005).
- ^[4]Edwards, G.S., Logan, R., Copeland, M. Reinisch, L., Davidson, J., Johnson, J. B, Maciunas, R. Mendenhall, M. Ossoff, R, Tribble, J, Werkhaven, J., and O'Day, D., "Tissue Ablation by a Free-Electron Laser Tuned to the Amide II Band," *Nature* 371, 416-419 (1994).
- ^[5]Hutson, M.S., Hauger, S.A., and Edwards, G., "Thermal Diffusion and Chemical Kinetics in Laminar Biomaterial Due to Heating by a Free-Electron Laser," *Physical Review E* 65: 061906 (2002).
- ^[6]Edwards, G.S., Pearlstein, R.D., Copeland, M.L., Hutson, M.S., Latone, K., Spiro, A., and Pasmanik, G., "6450-nm Wavelength Tissue Ablation Using a Nanosecond Laser Based on Difference Frequency Mixing and Stimulated Raman Scattering," *Optics Letters* 32, 1426-1428 (2007).
- ^[7]Hogenboom, D.O., DiMarzio, C.A., "Quadrature detection of a Doppler signal", *Applied Optics* Vol. 37, No. 13, May 1998.